Optical Networking With Variable-Code-Rate Transceivers

Darli A. A. Mello, *Member, IEEE*, André N. Barreto, *Senior Member, IEEE*,
Tiago C. de Lima, *Student Member, IEEE*, Thiago F. Portela, Lotfollah Beygi, and Joseph M. Kahn, *Fellow, IEEE*

***Abstract*—We evaluate the impact of variable-code-rate transceivers on cost, capacity and survivability of wavelength-routed optical networks. The transmission rate and reach trade-off is quantified for two hypothetical coded modulation schemes (aggressive and conservative) in a wavelength routing network with 50-GHz-spaced channels. The *aggressive scenario* assumes the 64-QAM modulation format, a small gap to capacity, and a small excess bandwidth. The *conservative scenario* considers the 16-QAM modulation format, and a larger capacity gap and excess bandwidth. The performance of the conservative and aggressive technologies is evaluated in three representative networks. Transparent reaches are calculated by means of an existing analytical method which assumes the AWGN hypothesis for the nonlinear noise. It is shown that variable-code-rate transceivers enable the concept of *soft protection*, in which the protection lightpath operates at a data rate which is lower than the corresponding working lightpath, in a way to avoid regeneration. This is specially attractive in the transport of IP traffic, where capacity reduction (in average up to 25%) may be tolerable during a repair time. It is also shown that variable-code-rate transceivers have the potential to offer significant savings in terms of transceiver usage and wavelength occupation, when compared to current fixed-rate transceivers operating at 100, 200 or 400 Gb/s. Finally, practical variable-code-rate transceivers may achieve a discrete set of N code rates, yielding a quantized capacity-*versus*-reach curve. The system impact of N is evaluated for several network scenarios.**

***Index Terms*—Coded modulation, optical communications, optical networking.**

I. Introduction

In recent years, optical transmission technology has advanced rapidly with the combination of multilevel modulation formats, coherent detection and digital signal processing algorithms. Optical systems at 100 Gb/s are widely available, and multiterabit superchannels have been demonstrated. While transmission technology is evolving to transfer higher data volumes over longer distances, optical networking is undergoing important changes to adapt to the new heterogeneous traffic demands. The most significant development in the network architecture is perhaps the introduction of the so-called flexible grid, in which the standard ITU-T channelization plan is replaced by a fine-granularity grid [1]. Proper use of the available network capacity, however, requires the effective combination of transmission and networking technologies.

Flexibility in the transmission reach can be achieved by varying three main parameters: symbol rate, modulation format, and code rate. The symbol rate is constrained not only by the bandwidth available to the channel but, mainly, by the capabilities of state-of-the-art analog-to-digital converters (ADCs). Thus, even if the flexible-grid technology allows the allocation of high-bandwidth channels (several hundreds of GHz), the limitations imposed by ADCs require encoding data in superchannels [2] to take benefit of the available spectrum. Under a fixed symbol rate (usually, the maximal allowed by ADCs), changing the modulation format also offers some flexibility. Current optical systems are able to switch among the 16-QAM, QPSK and BPSK modulation formats. In most of these systems, channel coding has been implemented using fixed-rate forward error correction (FEC). First- and second-generation systems use 7% overhead with hard decisions, while third-generation use 20% overhead with soft decisions. In systems using fixed-rate codes, reach has been extended by reducing the modulation format order, e.g., from 16-QAM to QPSK, with a two-fold reduction in the net transmission capacity. While the typical approach used in optical communications is to keep the code rate constant and change the constellation, other wired and wireless communication systems change both the code rate and the constellation [3], [4]. Some recent works on optical communications have used fixed constellations with variable-rate coding [5], or variable constellations with variable-rate coding [6], [7]. These used families of different low-density parity-check (LDPC) codes with different rates [6], [7] or Reed–Solomon codes of different rates derived from a single mother code by shortening and puncturing [5]. At high SNR, the performance of coded modulation is optimized if the constellation probability density function is two-dimensional Gaussian, which is known to be the capacity-achieving distribution. While this can be achieved using a constellation with unequally spaced points (geometric shaping) [8], it is considered more practical to use a set of equally spaced points with unequal probability [probabilistic shaping (PS)] [9].

Manuscript received April 18, 2013; revised November 11, 2013; accepted November 18, 2013. Date of publication November 21, 2013; date of current version December 11, 2013. At the University of Brasília, this work was supported by the Innovation Center, Ericsson Telecomunicações S.A., Brazil. At Stanford, this work was supported by a Google Research Award and by Corning, Inc.

D. A. A. Mello, A. N. Barreto, T. C. de Lima, and T. F. Portela are with the OCNLab, Department of Electrical Engineering, University of Brasília, Brasília DF 70910-900, Brazil (e-mail: darli@unb.br; andrebarreto@ene.unb.br; tiagolima@aluno.unb.br; thiagofport@unb.br).

L. Beygi was with the Department of Signals and Systems, Chalmers University of Technology, Göteborg 412 96, Sweden. He is now with Qamcom Research and Technology AB, 412 85 Göteborg, Sweden (e-mail: beygi@qamcom.se).

J. M. Kahn is with the E. L. Ginzton Laboratory, Department of Electrical Engineering, Stanford University, Stanford, CA 94305 USA (e-mail: jmk@ee.stanford.edu).

Color versions of one or more of the figures in this paper are available online at http://ieeexplore.ieee.org.

Digital Object Identifier 10.1109/JLT.2013.2292298

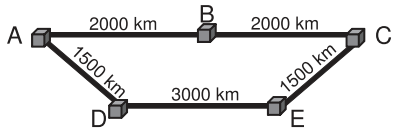

Fig. 1. Sample network.

TABLE I
SAMPLE TRANSPARENT REACHES

Data Rate	Transparent Reach
100 Gb/s	9.000 km
120 Gb/s	6.000 km
150 Gb/s	4.000 km
200 Gb/s	3.000 km

This paper evaluates the impact of variable-code-rate transceivers on cost, capacity and survivability of wavelength routed optical networks. To illustrate the problem, suppose that the operator of the network in Fig. 1 wishes to interconnect nodes A and C with 150 Gb/s, using optical transceivers with the transparent reaches in Table I. If fixed-code-rate transceivers are available at 100 or 200 Gb/s, two solutions are possible. The first one is routing a 200 Gb/s lightpath through route A-B-C with a regeneration point in B. The second option would be to use two unregenerated 100 Gb/s lightpaths. Alternatively, a variable-rate transceiver would enable setting up a single unregenerated 150 Gb/s lightpath. Suppose now that the connection in question carries critical IP traffic that needs protection. The fixed-code-rate solution would offer, again, two solutions with regenerators or extra wavelengths. The variable-code-rate alternative, though, allows the set up of a single unregenerated 120 Gb/s protection lightpath over route A-D-E-C. In this case there is, of course, a 20% capacity reduction in the protection lightpath, but this may be a tolerable degradation for contingency situations such as the repair of a fiber cut. We call the allocation of a lower capacity backup lightpath *soft protection*.

We perform analyses considering both conservative and aggressive technology scenarios representing current and near-future state-of-the-art technology. Fixed and variable-code-rate solutions are compared in three sample representative networks with different dimensions. Transparent reaches are calculated from the capacity curves obtained by the analytical model proposed in [10]. Practical implementations of variable-code-rate schemes may achieve a discrete set of code rates. The number of possible code rates, and the corresponding achievable rate-reach operating points, is limited by complexity constraints. Therefore, we also investigate the impact of the code-rate granularity on the system performance.

The rest of this paper is divided as follows. Section II presents the analytical model used to derive the aggressive and conservative technology scenarios investigated in the paper. Section III explains the network metrics used to compare the performance of different transceiver architectures. The simulation results are presented in Section IV. Finally, Section V concludes the paper.

TABLE II
TECHNOLOGY SCENARIOS

Parameter	Scenario	
	Aggressive	Conservative
Modulation Scheme	PM-64-QAM	PM-16-QAM
Coding Gap	1.25 dB	3 dB
Symbol Rate	44.4 Gbaud	40 Gbaud
Modulation	probabilistic shaping	uniform
SNR Margin	3 dB	3 dB
Maximal Bit Rate	533.33 Gb/s	320 Gb/s

II. TECHNOLOGY SCENARIOS

We evaluate the impact of variable-code-rate transceivers on optical networking based on the estimated transparent reach of optical links. In this section we describe how this reach is calculated in our work. We have considered two different technology scenarios. In the *aggressive scenario*, high-end technological advances, which are likely to be employed in the near future in transceiver architectures, are assumed. This includes high-resolution ADCs, which allow the use of higher-order modulation schemes up to 64-QAM; LDPC codes with long block lengths, and, consequently, small gap to capacity; and a small excess bandwidth, accounting for pulse shaping near the Nyquist limit. The *conservative scenario*, in turn, assumes the currently feasible technology, in which the ADC resolution limits the modulation scheme to 16-QAM; short codes with a larger gap are employed; and a larger excess bandwidth is required. The main parameters of both scenarios are summarized in Table II.

We wish to calculate the transparent reach for a given data rate R_b in bit/s, considering the aggressive and conservative scenarios. This is done in three steps. First, we obtain the minimum signal-to-noise ratio ($\mathrm{SNR}_{\mathrm{req}}$) required to allow the transmission of bit rate R_b with an arbitrarily low error rate. This is done using Shannon's capacity theorem, reviewed in Section II-A. The second step is to relate $\mathrm{SNR}_{\mathrm{req}}$ to the required optical signal-to-noise ratio $\mathrm{OSNR}_{\mathrm{req}}$, using a simple formula presented in [11]. Finally, the third step is to obtain the transparent reach L_{TOT} that yields $\mathrm{OSNR}_{\mathrm{req}}$.

The transparent reach calculation is based on the method proposed in [12], briefly reviewed in Section II-B, which models nonlinear distortions in optical links without chromatic dispersion compensation as AWGN. The accuracy of this assumption has been investigated by means of simulations [12] and experimental validation [13]. The calculation of the transparent reach requires the estimation of the optical launch power that maximizes the SNR of the link considering the interplay of optical power, amplified spontaneous emission (ASE) noise and nonlinear Gaussian-like noise. This optimal launch power depends on fiber type, amplifier properties and span length, but, for systems with incoherent noise accumulation, it is independent on the number of cascaded spans [12]. Thus, the calculation can be done using a single span. The method assumes that the accumulated ASE and nonlinear noise powers are proportional to the number of cascaded spans. Therefore, the maximal number of cascaded spans N_s is calculated as largest value that gives an OSNR greater than or equal to $\mathrm{OSNR}_{\mathrm{req}}$. The transparent reach

is the maximal number of spans multiplied by the span length. This analysis was initially performed in [10].

The derivations in [10] assume uniform QAM constellations with equiprobable symbols. However, longer transparent reaches may be achieved with unequally spaced points (geometric shaping) [8] or equally spaced points with unequal probability (PS) [9]. Both options impose a higher degree of complexity, but PS is considered to be more practical than geometric shaping. We adopt PS in the aggressive technology scenario according to the method explained in Section II-A.

A. Information-Theoretic Aspects

For a given discrete input alphabet with M complex elements A_k, the mutual information between channel input X and output Y, in bit/symbol, is given by [14]:

$$I(X;Y) = \sum_{k=0}^{M-1} \Pr(A_k) \int_{-\infty}^{\infty} p_{\mathrm{Y}|\mathrm{A}_k}(y|A_k) \cdot \log_2 \left[\frac{p_{\mathrm{Y}|\mathrm{A}_k}(y|A_k)}{\sum_{l=0}^{M-1} \Pr(A_l) p_{\mathrm{Y}|\mathrm{A}_l}(y|A_l)} \right] \mathrm{d}y \quad (1)$$

where $\Pr(A_k)$ is the probability of generating symbol A_k at the input; and $p_{\mathrm{Y}|\mathrm{A}_k}(y|A_k)$ is the probability density function of the channel output given that symbol A_k was transmitted. For a complex AWGN channel with noise variance σ^2 at each dimension, this pdf is given by:

$$p_{\mathrm{Y}|\mathrm{A}_k}(y|A_k) = \frac{1}{2\pi\sigma^2} e^{\frac{-|y-A_k|^2}{2\sigma^2}}. \quad (2)$$

Therefore, we look for the SNR $= E[|A_k|^2]/(2\sigma^2)$, here referred as $\mathrm{SNR}_{\mathrm{req}}$, which is required for a certain mutual information:

$$I(X;Y) = \frac{R_b}{R_s} \quad (3)$$

where R_b is the data rate whose transparent reach is being calculated, and R_s is the symbol rate in symbol/s determined by the technology scenario (aggressive or conservative).

In [10] and [14], it was considered that all symbols occur with the same probability. However, we can optimize $I(X;Y)$ choosing the input distribution that maximizes the mutual information $I(X;Y)$, i.e.,

$$C = \max_{\Pr(A_k)} I(X;Y). \quad (4)$$

We call C *constrained capacity*, since it is the maximal mutual information achieved by a specific modulation format. Constrained capacity may be approached by the Maxwell-Boltzmann distribution [9]:

$$\Pr(A_k) = \frac{1}{\sum_{A_k} e^{-\lambda|A_k|^2}} e^{-\lambda|A_k|^2}, \ \lambda \geq 0. \quad (5)$$

The constant λ has to be optimized numerically, and it varies with the SNR. We can vary the λ values and choose the one that maximizes the mutual information, and this has to be done for each SNR level, as it can be seen in Fig. 2. With PM-16-QAM, for example, the optimum values of λ can be seen in Fig. 3.

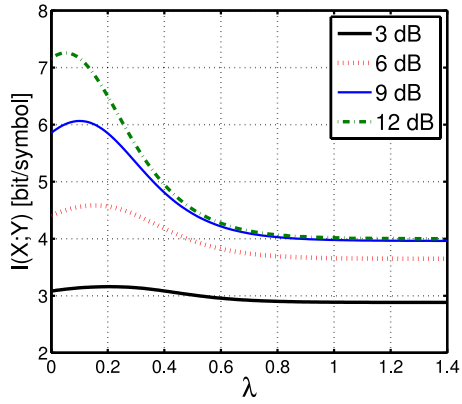

Fig. 2. Optimization of λ in the Maxwell–Boltzmann distribution for the PM-16-QAM modulation format.

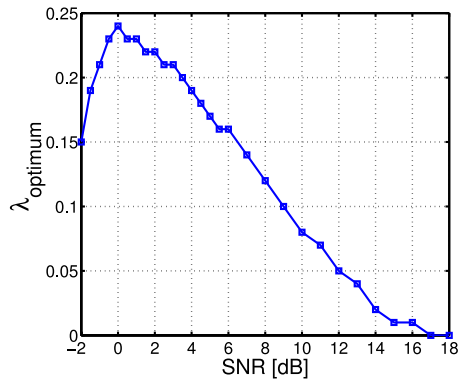

Fig. 3. Optimum values of λ for the PM-16-QAM modulation format.

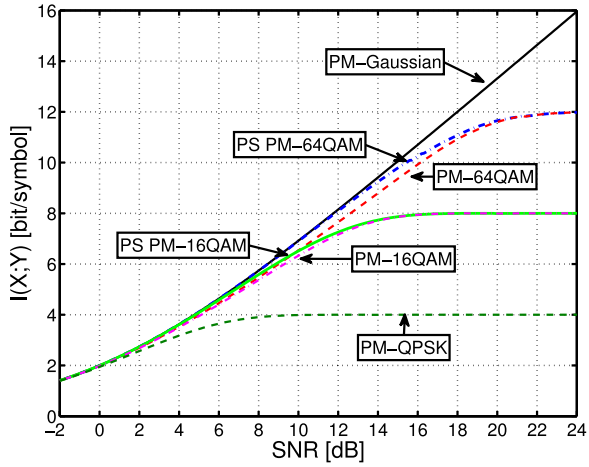

Fig. 4. Mutual information with different modulation schemes.

The PS gain, when compared with equiprobable constellation points, can be seen in Fig. 4, where we plot $I(X;Y)$ as a function of the SNR for different modulation schemes with polarization multiplexing (PM). We can clearly see that the use of PS allows us to approach the Shannon capacity for a Gaussian input at a wider SNR range than with equiprobable inputs. This figure motivates us to use higher-order modulation schemes with higher system redundancy overheads [7], [15], rather than low-order modulation formats with little redundancy, as it is

common in current optical networks. When using conventional FEC schemes, increasing coding overhead increases computational complexity. However, an appropriately designed coded modulation technique [15] can provide high performance with almost the same complexity for a wide range of spectral efficiencies. For example, if we want to transmit 7 bits/symbol we need nearly 1.5 dB less SNR with PM-64-QAM and a code rate $R = 7/12$ with PS, when compared to PM-16-QAM with $R = 7/8$.

In general the required number of dimensions to obtain the major part of shaping gain (around 1 dB) is much smaller than the number of dimensions needed for a channel coding scheme with a desirable performance [16]. Moreover, the decoder of a PS unit is usually implemented with a hard-decision-decoding method. Therefore, there is no significant increase in the system computational complexity due to adding PS. As explained earlier, a properly designed coded modulation scheme [15] can be exploited to construct a variable rate transceiver with negligible variation in the computational complexity for supporting different coding overheads. It is worth mentioning that the method proposed in [15] has lower hardware complexity (chip area) than techniques with either separate codes for each rate or deriving codes of all rates from a single mother code. Finally, the method proposed in [15] imposes the same system complexity (additional signaling or message transaction in the network) as conventional variable rate coding schemes.

Finally, we can relate required SNR and required OSNR as follows [11]:

$$\mathrm{SNR}_{\mathrm{req}} = \frac{2}{p}\frac{B_n}{R_s}\mathrm{OSNR}_{\mathrm{req}} \tag{6}$$

where p is the number of polarization modes and B_n the reference bandwidth.

B. Optical Channel Model With Non-Linear Interference

In coherent optical links without dispersion compensation, temporal dispersion causes the signal to be approximately Gaussian, and this approximation becomes more precise as the symbol rate increases and the links are longer, on account of the increased accumulated dispersion [17]. A consequence of this fact is that the non-linear interference can also be considered to be like AWGN. With these observations in mind, four-wave-mixing-like models were developed [12], [13]. These models slice the signal into different spectral components, assuming that they are statistically independent, and express analytically their nonlinear frequency beating to estimate the power spectral density $G_{\mathrm{NLI}}(f)$ of the non-linear interference. The description here follows the one proposed in [10].

With the AWGN assumption, we only need to calculate $G_{\mathrm{NLI}}(0)$, which, for a single span, is given by:

$$G_{\mathrm{NLI,SS}}(0) = \frac{16}{27}\gamma^2 G_{\mathrm{TX}}^3 \cdot \int_D \left| \frac{1-\mathrm{e}^{\left(j4\pi^2|\beta_2|f_1 f_2 - 2\alpha\right)L_s}}{2\alpha - j4\pi^2|\beta_2|f_1 f_2} \right|^2 \mathrm{d}f_1 \mathrm{d}f_2 \tag{7}$$

where γ is the fiber non-linearity coefficient ($\mathrm{W}^{-1}1/\mathrm{km}^{-1}$), α the fiber loss coefficient (km^{-1}), $|\beta_2|$ the absolute value of dispersion ($\mathrm{ps}^2\mathrm{km}^{-1}$), L_s the span length (km), and

$$G_{\mathrm{TX}} = \frac{P_{\mathrm{TX}}}{R_s} \tag{8}$$

the power spectral density of the transmitted signal, with P_{TX} the transmitted power and R_s the symbol rate.

This integral has to be performed numerically over the integration domain D, which depends on the number and occupation of the WDM channels, and on the symbol rate. For our choices of symbol rate, this domain is described in [12, Fig. 20].

The non-linear power in the optical reference bandwidth B_n (12.5 GHz) is given by:

$$P_{\mathrm{NLI,SS}} = G_{\mathrm{NLI,SS}}(0)B_n \tag{9}$$

and, from (8) and (7), we can rewrite (9) as

$$P_{\mathrm{NLI,SS}} = \eta_{\mathrm{SS}} P_{\mathrm{TX}}^3 \tag{10}$$

where η_{SS} is the non-linear coefficient:

$$\eta_{\mathrm{SS}} = \frac{16}{27}\gamma^2 \frac{B_n}{R_s^3} \cdot \iint_D \left| \frac{1-\mathrm{e}^{\left(j4\pi^2|\beta_2|f_1 f_2 - 2\alpha\right)L_s}}{2\alpha - j4\pi^2|\beta_2|f_1 f_2} \right|^2 \mathrm{d}f_1 \mathrm{d}f_2. \tag{11}$$

According to the experimental results in [12], non-linear noise accumulation can be expressed by the following equation:

$$G_{\mathrm{NLI}}(0) = G_{\mathrm{NLI,SS}}(0)N_s^{1+\epsilon} \tag{12}$$

where N_s is the number of spans and the coefficient ϵ typically lies between 0 and 0.6 [12]. If $\epsilon = 0$, the noise accumulation is fully incoherent and, if $\epsilon = 1$, the noise accumulation is fully coherent.

Supposing that the non-linear noise components from different spans add up incoherently, which is a reasonable assumption for a highly loaded spectrum, we can assume the total nonlinear noise to have a power:

$$P_{\mathrm{NLI}} = N_s P_{\mathrm{NLI,SS}}(0). \tag{13}$$

Consequently, a non-linear coefficient is given by:

$$\eta = N_s \eta_{\mathrm{SS}}. \tag{14}$$

The OSNR, including both ASE and non-linear noise, is given by:

$$\mathrm{OSNR} = \frac{P_{\mathrm{TX}}}{P_{\mathrm{ASE}} + P_{\mathrm{NLI}}} = \frac{P_{\mathrm{TX}}}{P_{\mathrm{ASE}} + \eta P_{\mathrm{TX}}^3}. \tag{15}$$

As the optical power increases, the SNR also increases if ASE only is considered, but the non-linear noise is enhanced. There is hence an optimal launch power that maximizes the OSNR:

$$P_{\mathrm{TX,OPT}} = \left(\frac{P_{\mathrm{ASE}}}{2\eta}\right)^{\frac{1}{3}}. \tag{16}$$

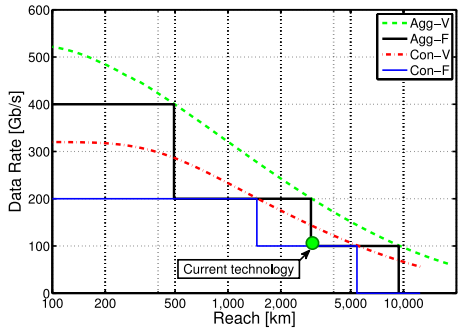

Fig. 5. Achievable data rate *versus* reach for fixed- (F) and variable-code-rate transceivers (V) using aggressive (Agg) and conservative (Con) technology.

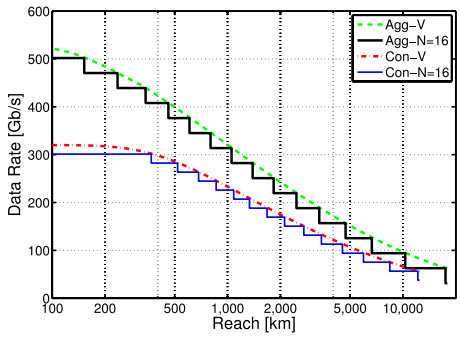

Fig. 6. Achievable data rate *versus* reach with 16 realizable code rates.

At the optimal optical power we can verify that the non-linear noise power is equal to half the ASE power, and, hence,

$$\mathrm{OSNR} = \frac{2P_{\mathrm{TX,OPT}}}{3P_{\mathrm{ASE}}} \tag{17}$$

where [10]:

$$P_{\mathrm{ASE}} = N_s F \left(e^{2\alpha L_s} - 1\right) h\nu B_n \tag{18}$$

with F the EDFA amplifier noise figure, h Plank's constant and ν the center frequency of the WDM comb.

From (18) and (17) we obtain the maximal number of spans as a function of the required $\mathrm{OSNR}_{\mathrm{req}}$:

$$N_s = \frac{2P_{\mathrm{TX,OPT}}}{3\mathrm{OSNR}_{\mathrm{req}} \cdot F\left(e^{2\alpha L_s} - 1\right) h\nu B_n} \tag{19}$$

and, consequently, the transparent reach is calculated as:

$$L_{\mathrm{TOT}} = N_s L_s. \tag{20}$$

The transparent reach varies as a function of the optical power for a fixed symbol rate and different channel spacing values Δf. As the ratio between the symbol rate and the channel spacing increases, the maximal reach decreases, on account of the increasing cross-channel interference. A thorough analysis of the transparent reach calculation, in different conditions, can be found in [10].

C. Rate-Versus-Reach Trade-off

Combining the analysis from Sections II-B and II-A we can obtain a relationship between the transparent reach, which corresponds to a certain $\mathrm{SNR}_{\mathrm{req}}$, as shown in (19) and (20), and the achievable data rate. In Fig. 5 we see how the achievable data rate varies as we increase the link distance considering the aggressive (Agg) and the conservative (Con) scenarios specified in Table II. The simulated fiber parameters are the same used in [10], i.e., standard single-mode fiber with attenuation constant $\alpha = 0.22$ dB/km, group velocity dispersion parameter $|\beta_2| = 21.7\ \mathrm{ps}^2/\mathrm{km}$ and nonlinear coefficient $\gamma = 1.27$ 1/W/km.

The coding gap and margin shown in Table II are added to $\mathrm{SNR}_{\mathrm{req}}$ as a system-specific penalty. The achievable data rates can be attained by employing variable-rate coding schemes, and in this figure we also plot the potential reach with fixed rates of 100, 200 and 400 Gb/s. It is clear that with variable-rate coding much higher transmission rates can be achieved at certain reaches. For instance, at 1000 km and with aggressive technology, the data rate can be increased from 200 Gb/s to over 300 Gb/s.

The *current technology* point corresponds to a 32-Gbaud PM-QPSK system using a FEC scheme presented in [18]. The scheme gives a net coding gain of 9.7 dB at a post-FEC BER of 1×10^{-15} and 20.5% overhead. The gap to Shannon capacity ($\mathrm{SNR}_{\mathrm{gap}}^{\mathrm{sc}}$) for a given coding scheme is obtained by:

$$\begin{aligned}\mathrm{SNR}_{\mathrm{gap}}^{\mathrm{sc}} = {} & 10\log_{10}\left\{[Q^{-1}(\mathrm{BER}_{\mathrm{ref}})]^2/2\right\} \\ & - 10\log_{10}(2^{2R} - 1) + 10\log_{10}(2R) - \mathrm{NCG}\end{aligned} \tag{21}$$

where NCG is the net coding gain at reference $\mathrm{BER}_{\mathrm{ref}}$, and R is the code rate. Code rate R and overhead OH are related by $R = 1/(1 + \mathrm{OH})$. Therefore, at the current technology point, the gap to Shannon capacity is 4.14 dB. However, the coding gap considered in our methodology (see Table II), $\mathrm{SNR}_{\mathrm{gap}}^{\mathrm{cc}}$, is computed with respect to the constrained capacity:

$$\mathrm{SNR}_{\mathrm{gap}}^{\mathrm{cc}} = \mathrm{SNR}_{\mathrm{gap}}^{\mathrm{sc}} - \Delta_{\mathrm{SNR}} \tag{22}$$

where Δ_{SNR} is the difference between the SNRs required to achieve a certain mutual information for the unconstrained and constrained cases (see Fig. 4). PM-QPSK modulation and a mutual information of 3.319 (4/1.205) bit/symbol yield $\Delta_{\mathrm{SNR}} = 1.15$ dB and, thus, $\mathrm{SNR}_{\mathrm{gap}}^{\mathrm{cc}} = 2.99$ dB. In addition to the coding gap, a 3-dB margin is also included, yielding a transparent reach of 3028.4 km.

Finally, it is important to point out that practical variable-code-rate transceivers may operate at a discrete set of rates because of complexity constraints. A finer granularity of rates allows a system to more closely approach the ideal rate-*versus*-reach trade-off. To investigate the impact of a discretized rate, we quantize the continuous rate-*versus*-reach curve into N equally spaced rates, as shown in Fig. 6 for $N = 16$.

III. Simulation Setup

We evaluate the impact of variable-code-rate transceivers on network cost and connectivity using four metrics: achievable data rate per connection, average number of transceivers per connection, distance blocking and average number of wavelengths per connection. All four metrics depend exclusively on

the rate-*versus*-distance curve (see Fig. 5) for each transceiver configuration, and on the network topology. Traffic issues are not investigated and left for a further study. Shortest paths are calculated using the Dijkstra algorithm applied to link lengths in kilometers.

A. Achievable Data Rate per Connection

This metric calculates the achievable data rate for a specific source-destination pair of the network. We use this metric to quantify, in case of *soft protection* (the allocation of a backup lightpath which has a lower capacity than the working lightpath), the achievable data rate in the working and protection lightpaths. The working lightpath takes the shortest path between a source-destination pair, and the protection lightpath the shortest path link-disjoint from the working path. In the example of Fig. 1, the achievable data rate of shortest path A-B-C is 150 Gb/s, and of protection path A-D-E-C 120 Gb/s.

B. Average Number of Transceivers per Connection

The number of transceivers per connection includes the devices in the source and destination nodes (two) and regeneration nodes (two per regenerator). Each connection is limited to a single wavelength (multiple wavelengths are not allowed). The average number of transceivers per connection metric is calculated over the shortest path of all source-destination pairs of the network. In our example in Fig. 1, the number of transceivers in path A-B-C would be two for a data rate of 100 Gb/s, and four at 200 Gb/s, because regeneration is needed in node B.

C. Distance Blocking

Distance blocking occurs when the achievable transparent reach of a transceiver is shorter than at least one link of the working path of a connection, i.e., the connection would be blocked even if regeneration was allowed. In the example of Fig. 1, distance blocking would occur in path A-D-E-C for data rates above 200 Gb/s, since link D-E would be longer than the transparent reach.

D. Average Number of Wavelengths per Connection

This metric is calculated under the assumption that regeneration is not allowed. It is, therefore, complementary to the average number of transceivers per connection. The data rate of a specific demand is fulfilled by the allocation of one or more unregenerated wavelengths. The average number of wavelengths per connection metric is computed over the shortest path of all source-destination pairs of the network. In the example of Fig. 1, the number of wavelengths per connection would be one for a data rate of 150 Gb/s, and two for 200 Gb/s (two unregenerated wavelengths at data rates below 150 Gb/s), because a single wavelength of 200 Gb/s would need regeneration in node B.

The four metrics are evaluated over the three sample networks (for further details, see [19]) shown in Figs. 7, 8 and 9 (distances appear in kilometers). Table III shows some topological parameters for the three networks under study. Each network link consists of 100-km spans of standard single-mode fiber (SSMF) carrying 79 wavelengths spaced by 50 GHz in the C-band. An odd number of wavelengths (79 instead of 80) is chosen to allow placing the test channel at the center of the spectrum. The fiber parameters used in the paper are the same assumed in [10].

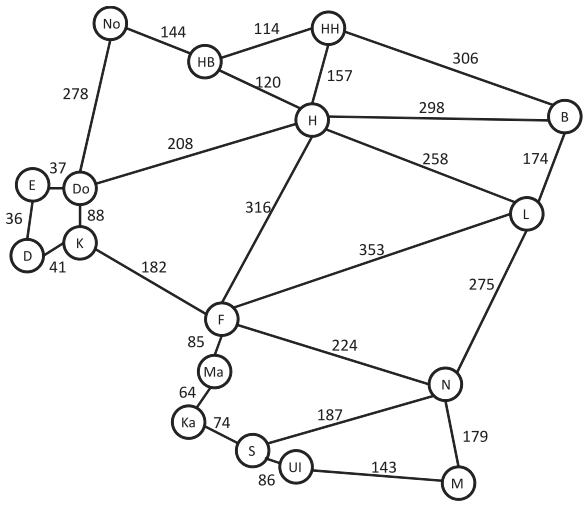

Fig. 7. German network.

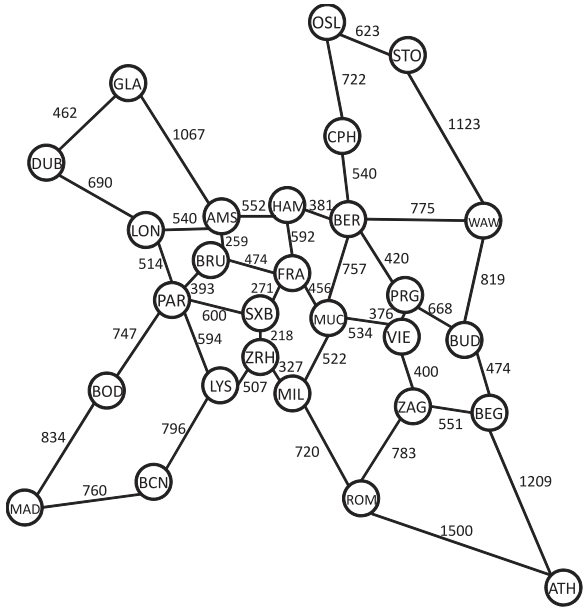

Fig. 8. European network.

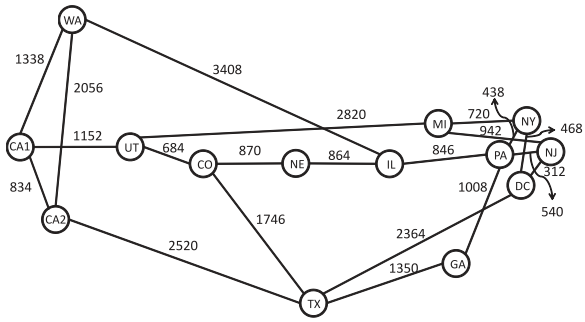

Fig. 9. American network.

TABLE III
TOPOLOGICAL PARAMETERS [19]

Network	German	European	American
Number of nodes	17	28	14
Number of links	26	41	21
Minimum link length (km)	36	218	312
Maximal link length (km)	353	1500	3408
Average link length (km)	170.3	625.4	1299.1

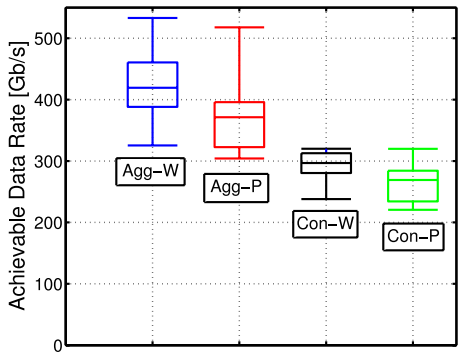

Fig. 10. Box plot of the achievable data rates in the German network, indicating the smallest observation (lowest dash), lower quartile (bottom of the rectangle), median (inside the rectangle), upper quartile (top of the rectangle), and largest observation (highest dash). Agg: aggressive technology; Con: conservative technology; W: working lightpath; P: protection lightpath.

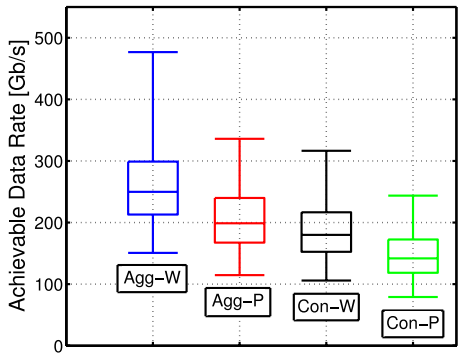

Fig. 11. Box plot of the achievable data rates in the European network, indicating the smallest observation (lowest dash), lower quartile (bottom of the rectangle), median (inside the rectangle), upper quartile (top of the rectangle), and largest observation (highest dash). Agg: aggressive technology; Con: conservative technology; W: working lightpath; P: protection lightpath.

IV. SIMULATION RESULTS

A. Achievable Data Rate per Connection and Soft Protection

We start with the evaluation of the *achievable data rate* (without regeneration) for all source-destination pairs in the German (see Fig. 10), European (see Fig. 11) and American (see Fig. 12) networks. The analysis is based on box plots indicating the smallest observation (lowest dash), lower quartile (bottom of the rectangle), median (inside the rectangle), upper quartile (top of the rectangle), and largest observation (highest dash). Four boxes are shown, corresponding to working and protection lightpaths for the aggressive and conservative technologies. The working lightpath takes the shortest path between a given source-destination pair, and the protection lightpath takes the shortest path which is link disjoint from the working lightpath.

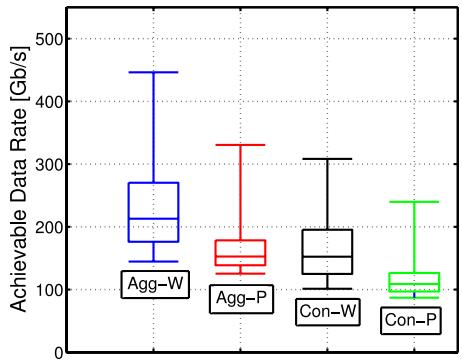

Fig. 12. Box plot of the achievable data rates in the American network, indicating the smallest observation (lowest dash), lower quartile (bottom of the rectangle), median (inside the rectangle), upper quartile (top of the rectangle), and largest observation (highest dash). Agg: aggressive technology; Con: conservative technology; W: working lightpath; P: protection lightpath.

TABLE IV
PENALTIES IN DATA RATE FOR THE PROTECTION LIGHTPATH WITH RESPECT TO THE WORKING LIGHTPATH

Network	Aggressive (%)	Conservative (%)
German	13.5	10.5
European	20.3	20.8
American	23.1	23.8

In the German network (see Fig. 10) and with aggressive technology, at least 300 Gb/s can be offered to any source-destination pair in the network for both the working and protection lightpaths. This is a strong indication of the benefits of the high data rate granularity provided by variable-code-rate transceivers compared to fixed-code-rate transceivers which, for example, work solely at 200 Gb/s or 400 Gb/s. Using conservative technology, about 50% of working lightpaths can be allocated at 300 Gb/s, but with protection lightpaths this amount is substantially lower. In the European network more than 50% of the working lightpath of all source destination pairs can be allocated with data rates between 200 Gb/s and 300 Gb/s, when using aggressive technology. With conservative technology, only some few 300 Gb/s connections can be allocated. In the American network, it is interesting to observe that, for conservative technology, the achievable data rate for 50% of the working lightpaths are well distributed between 100 Gb/s and 200 Gb/s, evidencing the benefits of variable-code-rate transceivers to fully exploit the link capacity. Table IV summarizes the average penalty in data rate for using the protection lightpath with respect to the working lightpath. The largest penalties are observed in the American network, with an almost 25% capacity reduction for the backup lightpath with aggressive and conservative technologies. This means that, in average, unregenerated *soft protection* can be implemented with approximately 25% data rate reduction.

B. Average Number of Transceivers per Connection and Distance Blocking

We evaluated the average number of transceivers per connection metric in the range of data rates where the variable-code-rate case with continous-valued data rates (Agg-V and Con-V) is free of distance blocking, which is the region of most interest.

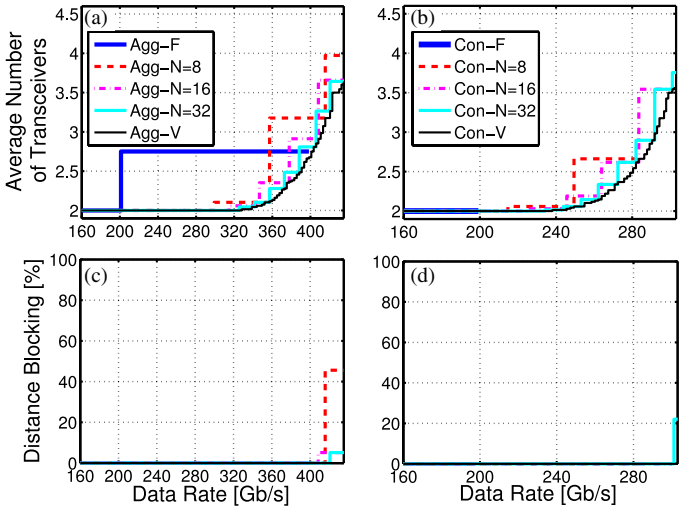

Fig. 13. German network analysis. Average number of transceivers per connection (a and b) and distance blocking (c and d) for the aggressive (a and c) and conservative (b and d) scenarios, with fixed code rates (F), and variable code rates with continuous- (V) or N-valued data rates (N).

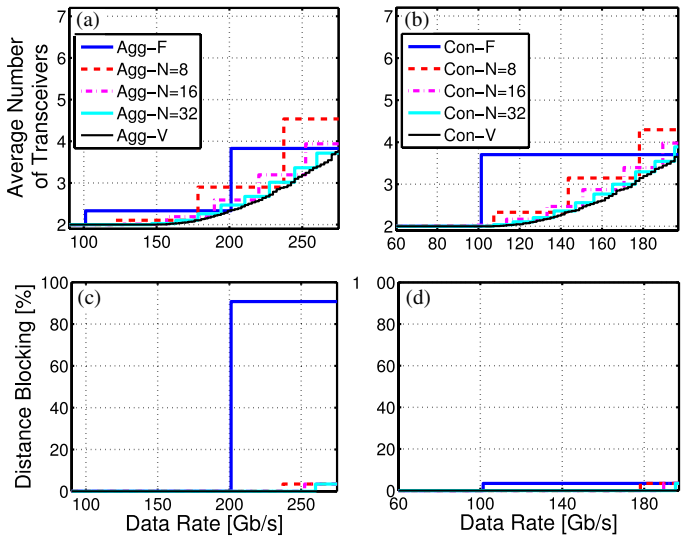

Fig. 14. European network analysis. Average number of transceivers per connection (a and b) and distance blocking (c and d) for the aggressive (a and c) and conservative (b and d) scenarios, with fixed code rates (F), and variable code rates with continuous- (V) or N-valued data rates (N).

Fig. 13 shows the average number of transceivers per connection and distance blocking for the German network. In the aggressive scenario (Fig. 13(a) and 13(c)), all source-destination pairs can be interconnected by a 200 Gb/s link without regeneration. Therefore, fixed or variable-code-rate technologies require the same number of transceivers. For data rates between 200 and 300 Gb/s, we find expressive savings when variable-code-rate transceivers are employed. Variable-code rate transceivers achieve 320 Gb/s with very little regeneration for $N \geq 8$. With conservative technology (Fig. 13(b) and 13(d)), regeneration is not required up to 200 Gb/s. With the fixed-code-rate option, transmission above 200 Gb/s is not possible because the maximal achievable bit rate is below 400 Gb/s. Variable-code-rate transmission enables a good range of operation between 200 Gb/s and 300 Gb/s with low distance blocking, with an increasing penalty with N. Distance blocking remained at low values for both aggressive and conservative technologies.

The results for the European network are shown in Fig. 14. In the aggressive scenario (Fig. 14(a) and 14(c)), for data rates in the 100-200 Gb/s range variable-code-rate transceivers exhibit an up to 14% reduction in the number of transceivers compared with the fixed-code-rate option. At data rates slightly higher than 200 Gb/s, the average number of transceivers with variable-code-rate transceivers ($N \geq 16$) is approximately 40% lower compared with the fixed-code-rate option. After 200 Gb/s, distance blocking increases sharply with fixed-code-rate transceivers. In the conservative scenario (Fig. 14(b) and 14(d)), for data rates up to 100 Gb/s, both transceivers offer the same average number of transceivers, and all connections do not need regeneration. Between 100 and 200 Gb/s, variable-code-rate transceivers show savings of up to 46%.

Fig. 15 presents the American network results. Link lengths in the American network are much longer than in the German and European networks. Thus, the average number of transceivers and distance blocking increase at even lower data rates. In the

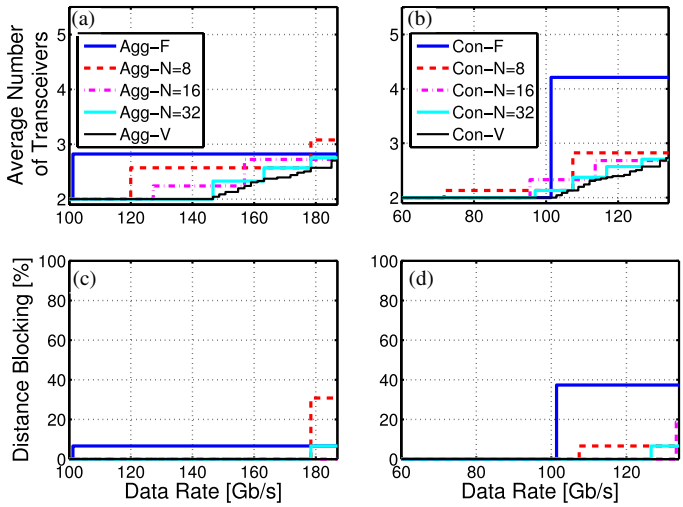

Fig. 15. American network analysis. Average number of transceivers per connection (a and b) and distance blocking (c and d) for the aggressive (a and c) and conservative (b and d) scenarios, with fixed code rates (F), and variable code rates with continuous- (V) or N-valued data rates (N).

aggressive scenario (Fig. 15(a) and 15(c)), variable-code-rate transceivers exhibit savings of up to 30% between 100 and 200 Gb/s. Over 200 Gb/s, distance blocking increases quickly for both aggressive and conservative technologies. In the conservative scenario (Figs. 15(b) and 15(d)), between 100 and 150 Gb/s, variable-code-rate transceivers offer savings of up to 50%. After 150 Gb/s, distance blocking increases abruptly for fixed and variable-code-rates.

C. Average Number of Wavelengths per Connection

The last investigated metric is the average number of lightpaths required to interconnect a source-destination pair without regenerators. Fig. 16 shows the results for the German network.

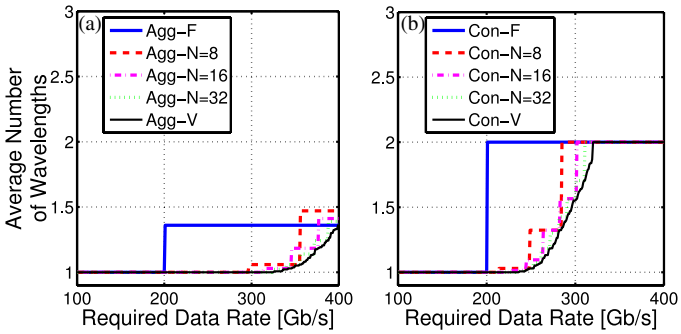

Fig. 16. German network analysis. Average number of wavelengths per connection for the aggressive (a) and conservative (b) scenarios, with fixed code rates (F), and variable code rates with continuous- (V) or N-valued data rates (N).

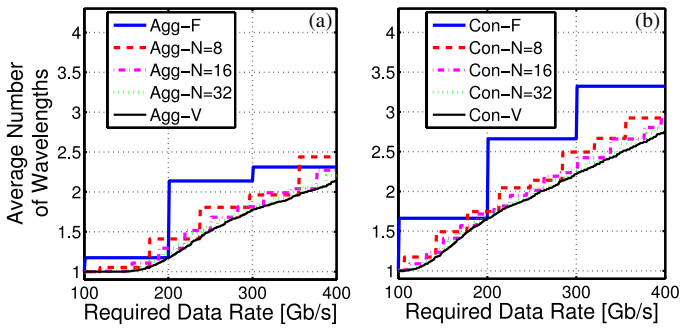

Fig. 17. European network analysis. Average number of wavelengths per connection for the aggressive (a) and conservative (b) scenarios, with fixed code rates (F), and variable code rates with continuous- (V) or N-valued data rates (N).

Using variable-code-rate transceivers, all source destination pairs can be interconnected by a single lightpath carrying up to ∼300 Gb/s (aggressive technology) or ∼200 Gb/s (conservative technology), respectively. If fixed-code-rate transceivers are used, data rates above 200 Gb/s require a second wavelength in both cases. The savings in using variable-code-rate transceivers reach 50% with the conservative technology and 25% with aggressive technology. The plateau in the variable-code-rate with conservative scenario curve can be explained by the fact that no more than two wavelengths are required to interconnect all source-destination pairs in the network. The results for the European network are presented in Fig. 17. In this case, the average number of wavelengths increases quasi-linearly to required data rate. Notice that plateaus, observed in the German network, do not appear, because the range of link distances in the European network is considerably larger. This heterogeneity of distances makes variable-code-rate transceivers specially interesting just after multiples of 100 Gb/s, because several source-destination pairs would require a new wavelength to obtain the transparent reach with fixed-code-rates. Fig. 18 presents the curves for the American network. Once again, the average number of wavelengths per connection metric becomes smoother with variable-code-rate transceivers, as N increases. The fixed-code-rate alternative, in turn, exhibits a few steps in multiples of 100 Gb/s.

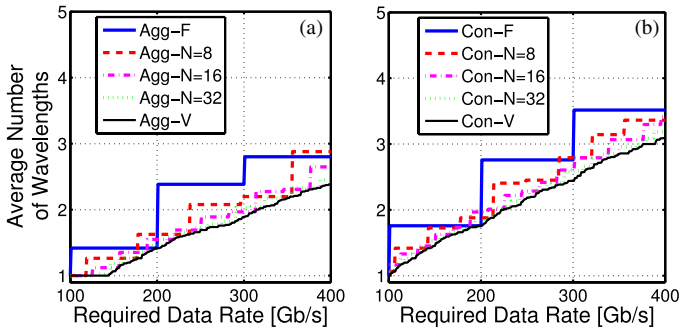

Fig. 18. American network analysis. Average number of wavelengths per connection for the aggressive (a) and conservative (b) scenarios, with fixed code rates (F), and variable code rates with continuous- (V) or N-valued data rates (N).

V. Conclusion

We investigated the impact of variable-code-rate transceivers on network-related metrics, and compared its performance with that of fixed-code-rate transceivers operating at the granularity of 100, 200 and 400 Gb/s. Two technology scenarios are used: a better-performing *aggressive technology* using the 64-QAM modulation format, PS and a lower gap to capacity provided by coding, and a worse-performing *conservative technology* with the 16-QAM modulation format and a larger gap to capacity. A 50-GHz wavelength grid was assumed. Both technology scenarios were applied to three sample network scenarios, a German, European and American networks. Variable-code-rate transceivers may achieve a discrete set of code rates. We also evaluated the impact of the number of realizable code rates N on the network performance. High gains in terms of cost and network occupancy were observed for variable-code-rate transceivers. The gains become more expressive with increasing N. In addition, we showed that variable-code-rate transceivers allow the deployment of what we called *soft protection*, where a lower capacity unregenerated protection lightpath is allocated to the working lightpath, avoiding regeneration. This technique has the potential to lower the costs of protection in networks carrying IP traffic, where a capacity degradation would be tolerable during fiber repairs. This capacity reduction varied in average from 10% to 25%.

References

[1] O. Gerstel, M. Jinno, A. Lord, and S. Yoo, "Elastic optical networking: A new dawn for the optical layer?" *IEEE Commun. Mag.*, vol. 50, no. 2, pp. 12–20, Feb. 2012.

[2] G. Bosco, V. Curri, A. Carena, P. Poggiolini, and F. Forghieri, "On the performance of Nyquist-WDM terabit superchannels based on PM-BPSK, PM-QPSK, PM-8QAM or PM-16QAM subcarriers," *J. Lightw. Technol.*, vol. 29, no. 1, pp. 53–61, Jan. 2011.

[3] S. Galli and O. Logvinov, "Recent developments in the standardization of power line communications within the IEEE," *IEEE Commun. Mag.*, vol. 46, no. 7, pp. 64–71, Jul. 2008.

[4] H. Holma and A. Toskala, *LTE for UMTS—OFDMA and SC-FDMA Based Radio Access*. Chippenham, U.K.: Wiley, 2009.

[5] G. H. Gho, L. Klak, and J. M. Kahn, "Rate-adaptive coding for optical fiber transmission systems," *J. Lightw. Technol.*, vol. 29, no. 2, pp. 222–233, Jan. 2011.

[6] M. Arabaci, I. Djordjevic, L. Xu, and T. Wang, "Nonbinary LDPC-coded modulation for rate-adaptive optical fiber communication without

bandwidth expansion," *IEEE Photon. Technol. Lett.*, vol. 24, no. 16, pp. 1402–1404, Aug. 2012.
[7] G. H. Gho and J. M. Kahn, "Rate-adaptive modulation and low-density parity-check coding for optical fiber transmission systems," *IEEE J. Opt. Commun. Netw.*, vol. 4, no. 10, pp. 760–768, Oct. 2012.
[8] G. Foschini, R. Gitlin, and S. Weinstein, "Optimization of two-dimensional signal constellations in the presence of Gaussian noise," *IEEE Trans. Commun.*, vol. COM-22, no. 1, pp. 28–38, Jan. 1974.
[9] U. Wachsmann, R. F. H. Fischer, and J. Huber, "Multilevel codes: Theoretical concepts and practical design rules," *IEEE Trans. Inf. Theory*, vol. 45, no. 5, pp. 1361–1391, Jul. 1999.
[10] G. Bosco, P. Poggiolini, A. Carena, V. Curri, and F. Forghieri, "Analytical results on channel capacity in uncompensated optical links with coherent detection," *Opt. Exp.*, vol. 19, no. 26, pp. 440–451, Dec. 2011.
[11] R.-J. Essiambre, G. Kramer, P. Winzer, G. Foschini, and B. Goebel, "Capacity limits of optical fiber networks," *J. Lightw. Technol.*, vol. 28, no. 4, pp. 662–701, Feb. 2010.
[12] P. Poggiolini, "The GN model of non-linear propagation in uncompensated coherent optical systems," *J. Lightw. Technol.*, vol. 30, no. 24, pp. 3857–3880, Dec. 2012.
[13] A. Carena, V. Curri, G. Bosco, P. Poggiolini, and F. Forghieri, "Modeling of the impact of nonlinear propagation effects in uncompensated optical coherent transmission links," *J. Lightw. Technol.*, vol. 30, no. 10, pp. 1524–1539, May 2012.
[14] G. Ungerboeck, "Channel coding with multilevel/phase signals," *IEEE Trans. Inf. Theory*, vol. 28, no. 1, pp. 55–67, Jan. 1982.
[15] L. Beygi, E. Agrell, J. M. Kahn, and M. Karlsson, "Rate-adaptive coded modulation for fiber-optic communications," *J. Lightw. Technol.*, DOI 10.1109/JLT.2013.2285672, 2013.
[16] J. G. D. Forney and G. Ungerboeck, "Modulation and coding for linear Gaussian channels," *IEEE Trans. Inform. Theory*, vol. 44, no. 6, pp. 2384–2415, Oct. 1988.
[17] L. Beygi, E. Agrell, P. Johannisson, M. Karlsson, and H. Wymeersch, "A discrete-time model for uncompensated single-channel fiber-optical links," *IEEE Trans. Commun.*, vol. 60, no. 11, pp. 3440–3450, Nov. 2012.
[18] F. Chang, K. Onohara, and T. Mizuochi, "Forward error correction for 100 G transport networks," *IEEE Commun. Mag.*, vol. 48, no. 3, pp. S48–S55, Mar. 2010.
[19] A. Betker, C. Gerlach, R. Hülsermann, M. Jäger, M. Barry, S. Bodamer, J. Späth, C. Gauger, and M. Köhn, "Reference transport network scenarios," MultiTeraNet Rep., Jul. 2003.

Darli A. A. Mello studied electrical engineering at the RWTH-Aachen, Aachen, Germany, and at the State University of Campinas (UNICAMP), Campinas, Brazil, where he graduated in 2000. He received the M.Sc. degree from the Institute for Communications Engineering, Munich University of Technology, Munich, Germany, in 2002. During his Master's studies, he carried out both experimental and theoretical work at the Siemens research labs in Munich. He received the Ph.D. degree from UNICAMP, in 2006.

After his Ph.D. studies, he joined Padtec Optical Components and Systems as a Senior Technology Engineer. There, he was responsible for R&D project coordination, system conception and design, and for cooperative projects with universities. Since August 2008, he has been with the Department of Electrical Engineering, University of Brasilia, Brasilia, Brazil, as an Assistant Professor. His main research interests include architecture of optical transceivers and networks.

Dr. Mello was the TPC Co-Chair of the 30th Brazilian Telecommunications Symposium, 2012, and is part of subcommittee 12 (core networks) of OFC.

André N. Barreto graduated in electrical engineering from Catholic University, Rio de Janeiro, Brazil, in 1994, where he also received the Master's degree in 1996. He received the Dr.Ing. degree with highest honours (*summa cum laude*) from the Dresden University of Technology, Dresden, Germany, in 2001.

Since 2009, he has been an Assistant Professor at the University of Brasília, Brasília, Brazil. He also held positions previously at the IBM Research Center in Zurich, Switzerland, at Claro, in Rio de Janeiro, and at the Nokia Institute of Technology, in Brasília. He is the author of four international patents and numerous articles in journals and in international conferences. His current areas of interest are broadband wireless communication systems PHY and MAC, spectrum sensing for cognitive radio, and transmission techniques for advanced optical communication systems.

Tiago C. de Lima has a degree in electrical engineering from the University of Brasília, Brasília, Brazil, in 2012, where he is currently working toward the Master's degree.

He was a Trainee at Globo TV network and spent six months as an exchange student at the University of Coimbra, Coimbra, in Portugal. He is the current Vice-chair of IEEE-GOLD at Centro-Norte Brazil Section. His research interests are in error-correcting codes and link adaptation for optical networks.

Thiago F. Portela received degrees in mathematics from the State University of Goias, Goias, Brazil, in 2006, and in communication networks engineering from the University of Brasilia, Brasilia, Brazil in 2010, where he also received the Master's degree in electrical engineering in 2013.

His main research interests include digital signal processing for next-generation optical transceivers.

Lotfollah Beygi received the Ph.D. degree from the Chalmers University of Technology, Göteborg, Sweden, in 2013.

He was with the R&D division of Zaeim Electronic Industries from 2003 to 2008. He is currently with Qamcom Research & Technology AB, Göteborg. His main research interests include coded modulation and digital signal processing for fiber-optical and wireless communications.

Joseph M. Kahn received the A.B., M.A., and Ph.D. degrees in physics from University of California, Berkeley, Berkeley, CA, USA (U.C. Berkeley) in 1981, 1983, and 1986, respectively.

From 1987–1990, he was at AT&T Bell Laboratories, Crawford Hill Laboratory, in Holmdel, NJ, USA. He demonstrated multi-Gbit/s coherent optical fiber transmission systems, setting world records for receiver sensitivity. From 1990–2003, he was in the faculty of the Department of Electrical Engineering and Computer Sciences at U.C. Berkeley, performing research on optical and wireless communications. Since 2003, he has been a Professor in the Department of Electrical Engineering, Stanford University, Stanford, CA, USA, where he heads the Optical Communications Group. His current research interests include fiber-based imaging, spatial multiplexing, rate-adaptive and spectrally efficient modulation and coding methods, coherent detection and associated digital signal processing algorithms, digital compensation of fiber nonlinearity, and free-space systems. In 2000, he helped found StrataLight Communications, where he served as Chief Scientist from 2000–2003. StrataLight was acquired by Opnext, Inc. in 2009.

Dr. Kahn received the National Science Foundation Presidential Young Investigator Award in 1991. From 1993–2000, he served as a Technical Editor of *IEEE Personal Communications Magazine*. Since 2009, he has been an Associate Editor of the IEEE/OSA JOURNAL OF OPTICAL COMMUNICATIONS AND NETWORKING.